

First principles study of the origin and nature of ferromagnetism in (Ga,Mn)As

Stefano Sanvito*

Materials Department, University of California, Santa Barbara, CA 93106, USA

Pablo Ordejón

Institut de Ciència de Materials de Barcelona (CSIC) Campus de la U.A.B, E-08193 Bellaterra, Barcelona, Spain

Nicola A. Hill

Materials Department, University of California, Santa Barbara, CA 93106, USA

(Dated: October 28, 2018)

The properties of diluted $\text{Ga}_{1-x}\text{Mn}_x\text{As}$ are calculated for a wide range of Mn concentrations within the local spin density approximation of density functional theory. Mülliken population analyses and orbital-resolved densities of states show that the configuration of Mn in GaAs is compatible with either $3d^5$ or $3d^6$, however the occupation is not integer due to the large p - d hybridization between the Mn d states and the valence band of GaAs. The spin splitting of the conduction band of GaAs has a mean field-like linear variation with the Mn concentration and indicates ferromagnetic coupling with the Mn ions. In contrast the valence band is antiferromagnetically coupled with the Mn impurities and the spin splitting is not linearly dependent on the Mn concentration. This suggests that the mean field approximation breaks down in the case of Mn-doped GaAs and corrections due to multiple scattering must be considered. We calculate these corrections within a simple free electron model and find good agreement with our *ab initio* results if a large exchange constant ($N\beta = -4.5\text{eV}$) is assumed.

PACS numbers: 75.50.Pp, 75.30.Et, 71.15.Mb, 71.15.Fv

I. INTRODUCTION

The discovery of ferromagnetic order in diluted magnetic semiconductors (DMS) made of heavily Mn-doped InAs [1] and GaAs [2, 3, 4] paves the way for many new semiconductor spin-devices [5]. In particular the ferromagnetism of $\text{Ga}_{1-x}\text{Mn}_x\text{As}$ adds the spin degree of freedom to the GaAs/(Al,Ga)As system which, in the last few years, has been the benchmark for new physics and for high speed electronic and optoelectronic devices.

Long spin-lifetime [6] and spin-coherence [7] in GaAs have already been demonstrated. Recently the feasibility of spin-injection into GaAs using (Ga,Mn)As contacts has been proved [8] overcoming the intrinsic difficulty of injecting spins into semiconductors from magnetic metals [9]. These two effects suggest that the GaAs/(Al,Ga)As/(Ga,Mn)As system is the best candidate for injecting, storing and manipulating spins in entirely solid state devices; a valuable step towards a practical realization of quantum computing [10].

Although there is general agreement on the carrier-(hole-) mediated origin of the ferromagnetism in (Ga,Mn)As, the detailed mechanism is still a matter of debate [11, 12, 13]. Recently Dietl *et al.* studied the ferromagnetism of III-V DMS within the Zener model,

and obtained good agreement with existing experimental data using few phenomenological parameters. One of the key elements of the model is the mean-field Kondo-like coupling (p - d Hamiltonian) between the valence band of the host semiconductor and the magnetic impurity

$$H_{sp-d} = -N\beta\vec{s} \cdot \vec{S}, \quad (1)$$

where $N\beta$ is the p - d exchange constant, \vec{s} is the valence band electron spin and \vec{S} is the impurity spin. In this model the exchange constant, which governs the spin splitting of the valence band of the host semiconductor, enters quadratically in the expression for the Curie temperature. Therefore its exact evaluation is crucial for making quantitative predictions about the ferromagnetism in both existing and novel materials.

Unfortunately, in contrast with the case of II-VI DMS's, the experimental determination of $N\beta$ is not conclusive, and both the sign and the magnitude are not well known, particularly for large Mn concentrations ($x > 0.01$). From the exciton splitting in the low dilution limit ($x < 0.001$) the coupling is found to be ferromagnetic with an exchange constant of $N\beta = +2.5\text{eV}$ [14], if the exchange constant for the conduction band $N\alpha$ is assumed to be $+0.2\text{eV}$ (a typical value for Mn in II-VI semiconductors). Reflectance magnetic circular dichroism [15] and magnetoabsorption experiments [16] present controversial results since the absorption edge splitting is strongly dependent on the hole concentration (Moss-Burstein effect), which in turn is difficult to determine

*Electronic address: e-mail: ssanvito@mrl.ucsb.edu

from transport measurements because of a strong magnetoresistance up to very high magnetic fields [3]. Magnetotransport experiments are able to measure only the magnitude of the exchange constant and the values obtained vary from $|N\beta|=3.3$ eV [17] to $|N\beta|=1.5$ eV [18]. Finally a recent core-level photoemission study [19] of $\text{Ga}_{0.926}\text{Mn}_{0.074}\text{As}$ gives $N\beta=-1.2$ eV if the Mn^{2+} configuration is assumed. Nevertheless it is worth noting that the raw data are compatible with both the Mn^{2+} and the Mn^{3+} configurations and so one cannot make a definite determination of the sign of $N\beta$.

From a theoretical point of view, the exchange interaction for the conduction band results from a direct coulombic exchange and is expected to be ferromagnetic. In contrast the exchange interaction of the valence band has a kinetic energy origin. It can be described as a virtual process in which electrons from the valence band jump onto the localized $3d$ states of Mn [20]. Therefore the sign and strength of the coupling depend critically on the population of the spin-polarized Mn d -orbitals. For less than half-filled d -orbitals Hund's rules suggest that the coupling is ferromagnetic; for half- and more than half-filling the coupling is antiferromagnetic. In this respect the case of Mn is rather peculiar. Three types of Mn centers in GaAs are possible. The first two can be seen as substitutional Mn^{3+} and Mn^{2+} respectively, with the former neutral (A^0 with formal $3d^4$ configuration) with spin $S = 2$ and the latter negatively charged (A^- with formal configuration $3d^5$) with spin $S = 5/2$. The third center is obtained when A^- weakly binds a hole, forming a neutral ($3d^5+h$) complex. The A^- center provides only antiferromagnetic coupling with the valence band, while the neutral A^0 centers can provide either ferromagnetic or antiferromagnetic. The ferromagnetic coupling can arise both from the half-filled $3d^4$ center and by hopping through the spin polarized bound hole in the ($3d^5+h$) case [21].

From this brief overview it is clear that a detailed description of the electronic structure of Mn in GaAs is crucial for understanding and modeling correctly the ferromagnetism of $\text{Ga}_{1-x}\text{Mn}_x\text{As}$. In this paper we address this issue by calculating the ground state properties of (Ga,Mn)As over a range of Mn concentrations using density functional theory (DFT) [22] in the local spin density approximation (LSDA). We use a numerical implementation of DFT based on pseudopotentials and pseudo-atomic orbitals [23, 24, 25]. Although the convergence versus basis set with localized orbitals is more difficult than with plane waves (where a single parameter, the energy cutoff, determines the completeness of the basis), the method has the great advantage of being able to handle a large number of atoms with an accuracy comparable to plane-waves methods. This allows us to investigate various Mn dilutions without the need of large computer resources. Moreover the pseudo-atomic basis

is very convenient for analysis of atomic occupation and orbital-resolved DOS, since no overlap integrals between different bases have to be calculated.

The remainder of this paper is organized as follows. In the next section we provide some technical details about the calculation method, illustrating in particular how to optimize the pseudo-atomic basis set. Then we present our results for $\text{Ga}_{1-x}\text{Mn}_x\text{As}$ for Mn concentrations ranging from $x = 1$ to $x = 0.02$. We analyze the density of states projected onto the different orbital components, the charge distribution around the Mn ions and we perform Mülliken population analyses to determine the occupation of the d -orbitals of Mn. In section IV we discuss the p - d exchange constant and we compare our results with that expected from the Kondo-like effective Hamiltonian (1) in the mean field approximation. Then we illustrate how the mean field picture breaks down in the case of Mn in GaAs and how the LDA results can be explained by a simple model which includes multiple scattering contributions. Finally in section VI we present our conclusions.

II. COMPUTATIONAL TECHNIQUE

Since we are interested in the calculation of the electronic properties of diluted alloys systems, we need a method that is able to handle with sufficient accuracy a large number of atoms within a periodic supercells approach. To that purpose, we use a DFT approach based on pseudopotentials, and numerical localized atomic orbitals as basis sets. This method, implemented in the code SIESTA [23, 24, 25], combines accuracy and a small computational cost compared to other approaches with considerably larger computational requirements, such as plane waves. In this approach, however, special care must be devoted to the optimization of the basis set, in order to obtain the desired accuracy. In this section, we describe the optimization procedure used in this work. For all the DFT calculations presented here, we use the Ceperley-Alder [26] form of the exchange-correlation potential. Self-consistency is achieved using the Pulay density mixing scheme [27], with a convergence criterion of 10^{-6} for the change in the elements of the density matrix.

A. Pseudopotentials

We use the widely used scalar relativistic Troullier-Martins pseudopotentials [28] with non linear core corrections [29] and Kleinman-Bylander factorization [30]. The reference configurations are $4s^24p^03d^5$, $4s^24p^33d^0$ and $4s^24p^13d^0$ respectively for Mn, As and Ga. The cutoff radii for the s , p and d components of the pseudopotential are: 1)Mn 2.00, 2.20 and 1.90 au, 2)As 1.90,

2.20 and 2.50 au and 3)Ga 2.10, 2.50 and 3.0 au. We check the pseudopotentials at the atomic level by comparing the pseudoeigenvalues with those generated by all electron calculations for several atomic and ionic configurations.

In order to check the transferability of the pseudopotentials just described, we have chosen to use a plane waves method [31]. This allows us to perform essentially converged calculations with respect to the basis set (by using a sufficiently large energy cutoff for the plane waves). This would be difficult with the local orbitals, since basis set convergence is much more problematic and complicated in that case. In that way, we isolate pseudopotential effects from basis set effects in checking the pseudopotential. We have computed the equilibrium lattice constant and the band structures of both GaAs and MnAs, both of them showing good agreement with previously published results [32].

After testing the pseudopotential, we have also calculated the band structure for a fixed localized orbitals basis set over a range of pseudopotentials cutoff radii. Our results show that, as expected, the pseudopotentials that yield the best results with plane waves also gives the best band structures with the localized atomic orbitals.

B. Basis set: Number of ζ 's

Let us now turn our attention to the pseudoatomic basis set. The procedure to generate the numerical atomic orbitals is described in Ref. 33. The atomic orbitals are constructed as the product of an angular function with a given angular momentum l (yielding to s -type, p_x, p_y, p_z -type, etc. orbitals), and a numerical radial function. Several functions with the same angular and different radial form can be considered to represent the same atomic shell, referred to as multiple- ζ functions. The radial functions are determined as follows: the first ζ 's are obtained according to the scheme proposed by Sankey and Niklewski [34], as the confined pseudo-atomic orbitals (PAO's) which result from the DFT solution of the free atom with the pseudopotential, and spherical potential of radius r_c . The pseudo-wavefunction $\phi(r)$ constructed in such a way extends only to distances smaller than the cutoff radius r_c . Note that this does not correspond to a simple truncation, since the pseudo-wavefunction is continuous at $r = r_c$. The second and successive ζ 's are constructing in the split-valence spirit. They are obtained by subtracting from the first ζ a function which reproduces the tail of the pseudoatomic orbital for $r > r_{\text{DZ}}$ and continues towards the origin as $r^l(a - br^2)$. Here l is the angular momentum, a and b are parameters chosen to ensure the continuity, and DZ refers to "double- ζ ". r_{DZ} is chosen in such a way that the total norm beyond this radius has a certain value. In the present calculation we

always fix the norm beyond r_{DZ} to 15% of the total norm, having noted that small variations around that value do not produce any significant changes in the total energy. Further ζ 's are calculated by repeating the same scheme. This approach is more efficient than using excited states of the neutral atom, which can be unbound [33].

The optimization of the PAO basis is more delicate than that of its plane-wave counterpart, where a single parameter (the energy cutoff) determines the accuracy and completeness of the basis. In the case of the PAO bases used here, several parameters determine the accuracy of the basis: the number of ζ 's for each shell, the angular momentum components included, the confinement radii, etc. All these must be optimized to achieve the required accuracy. As well as in plane-waves, more complete bases produce more accurate results, but also require larger computational resources. Since we are interested in describing the magnetic properties of (Ga,Mn)As, it is natural to choose a magnetic quantity as the one to monitor the convergence of our results with respect to the basis set quality. We study the energy difference Δ_{FA} between the ferromagnetic and antiferromagnetic alignments of two Mn atoms in a four atom unit cell of zincblende MnAs as a function of the basis set. The lattice constant is chosen to be $a_0 = 5.8\text{\AA}$, which is the critical lattice constant for the half metallic behavior of MnAs [32].

The first problem we address is the number of ζ 's to include for each atomic orbital. We start by choosing double- ζ for the s orbitals of both Mn and As and single- ζ for the p orbitals and for the d orbitals of Mn, then progressively increase the number of basis orbitals. The initial cutoff radii are chosen as indicated in table I and are proportional to the positions of the maxima of the unconstrained pseudo-wave-functions. In figure 1 we present

Orbital	r_c (au)
Mn s	6.0
Mn p	6.0
Mn d	5.0
As s	5.5
As p	5.5

TABLE I: Initial cutoff radii used for fixing the number of ζ 's. The radii are given in atomic unit.

the total energies for the ferromagnetic (E_{FM}) and antiferromagnetic (E_{AF}) alignments, and Δ_{FA} , for the different PAO bases listed in table II. From the picture two important conclusions can be reached. First, according to the usual variational principle the total energies for both ferromagnetic and antiferromagnetic configurations decrease with enlarging the basis. Second the split between the ferromagnetic and antiferromagnetic configurations is significantly reduced by using triple- ζ 's for the

Basis	$N_\zeta(\text{As } s)$	$N_\zeta(\text{As } p)$	$N_\zeta(\text{Mn } s)$	$N_\zeta(\text{Mn } p)$	$N_\zeta(\text{Mn } d)$
1	2	1	2	1	1
2	2	1	2	1	2
3	2	1	2	2	2
4	2	2	2	2	2
5	2	2	2	2	3
6	2	2	3	2	3
7	2	3	2	2	3
8	2	2	2	3	3

TABLE II: Summary of the bases used in figure 1. In the first column the indicator of the basis, the following columns show the number of ζ (N_ζ) for each orbital.

d orbitals of Mn (note the large decrease of Δ_{FA} when going from basis 1 to basis 2 and from basis 4 to basis 5) and double- ζ for the p orbitals of As. This sensitivity of

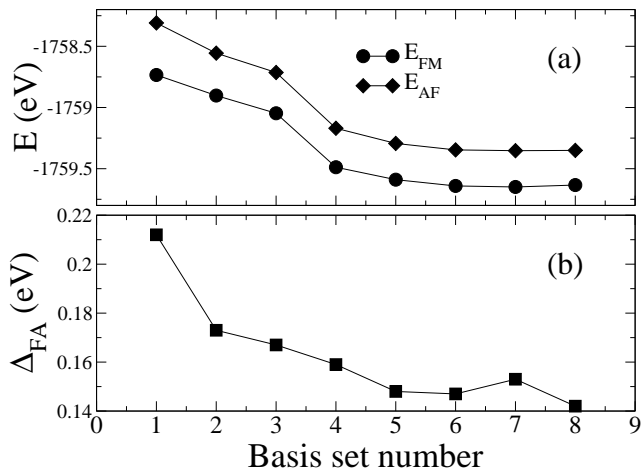


FIG. 1: (a) E_{FM} , E_{AF} and (b) Δ_{FA} for the basis of table II. Note the decreasing of the total energies as the basis becomes more complete. Δ_{FA} saturates for the basis 5.

the magnetic phase stability to the As- p and Mn- d basis is consistent with the magnetism in MnAs being driven by strong p - d hybridization. Since we are mainly interested in the magnetic properties of diluted systems describable by very large unit cells we decide to use double- ζ for all the orbitals except the d orbitals of Mn for which we use triple- ζ (this is the fifth basis set in table 2). Note that we can afford to use triple- ζ for Mn- d since few Mn ions are present in the cell. In contrast the use of larger basis sets for Ga and As yields a more dramatic increase of the size of the computations.

C. Basis set: Cutoff radii

Next we turn our attention to the choice of the cutoff radii of the basis sets. For free atoms, the optimum cutoff radius of any orbital (as the one which minimizes the energy) is infinite, since that case corresponds to no confinement potential, which yields to exponential tails for all the atomic wavefunctions. However, in solids this criterion does not hold, since the lack of vacuum and the presence of the crystal potential tend to confine the atomic wavefunctions more than in the free atom. In this situation, the confinement of each PAO should be optimized to minimize the total energy. This procedure has shown in other systems like bulk bcc Fe [35] that a finite and relatively small confinement radius can provide lower energies and therefore more accurate bases than long values of r_c . These calculations also show that the optimum confinement radius of each PAO depend very much on the particular orbital. In our case, however, it would be too complex to optimize the r_c for all the orbitals in our system, due to the large number of them. Instead, we have followed a simpler approach. We vary the cutoff radii of table I uniformly by multiplying all the radii by a common scaling factor t . A somewhat similar criterion is to use as variational parameter the orbital energy shift ΔE_{PAO} , which is the energy increase that each orbital experiences when confined to a finite sphere and can be used as single parameter to test the convergence [33].

In figure 2 we present E_{FM} , E_{AF} and Δ_{FA} as a function of t for the fifth basis set of table 2. The last point

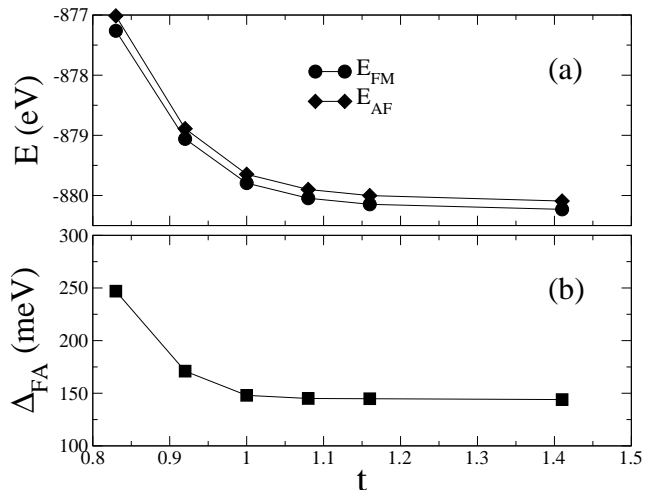


FIG. 2: (a) E_{FM} , E_{AF} and (b) Δ_{FA} for the fifth basis set of table II as a function of the scaling parameter t . Note that Δ_{FA} saturates sooner than the total energies for ferromagnetic and antiferromagnetic alignment.

in figure 2 ($t = 1.41$) corresponds to a basis with an

orbital energy shift ΔE_{PAO} of 0.001Ry. A convergence of 0.001Ry has been successfully used to describe the magnetic properties of Ni clusters on Ag surfaces [36] and is considered an optimal value for the convergence. However in our case we prefer to use smaller cutoff radii in order to reduce the computation time. From figure 2 it is clear that the saturation of Δ_{FA} occurs for shorter radii than those required to converge the total energies. We therefore decide to fix the cutoff radii to $t = 1$ noting that E_{FM} and E_{AF} differ from the value obtained for $\Delta E_{\text{PAO}}=0.001\text{Ry}$ by only 0.04% and that Δ_{FA} differs by only 2%.

D. Comparison with previous calculations

We further test our basis set by computing the energy split between the Mn d states with e and t_2 symmetry at the Γ point, and the dependence of the magnetization on the lattice spacing for zincblende MnAs. These two tests give an indication of the accuracy of the p - d exchange, which is a dominant interaction in (Ga,Mn)As. In fact at the Γ point the t_2 states are coupled with the As- p states while the e are decoupled, and their splitting is determined by the p - d coupling.

In figure 3 we present the energy split $\Delta E_{e-t_2} = E_e - E_{t_2}$ as a function of t for both the spin directions. The e - t_2 split converges monotonically and there is a

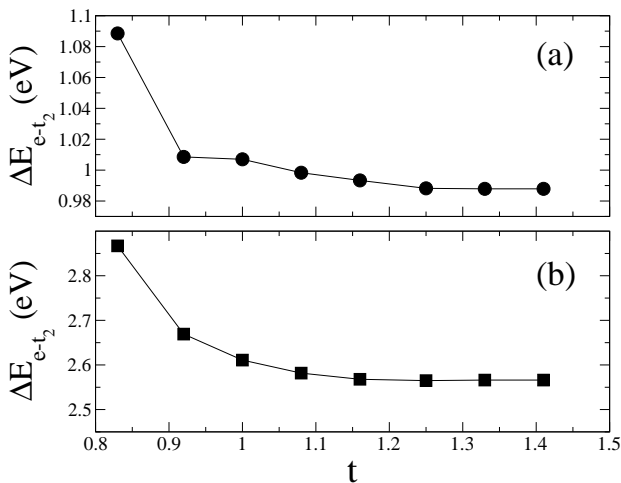


FIG. 3: e - t_2 energy split at the Γ point for MnAs: (a) majority spin, (b) minority spin.

variation of only $\sim 2\%$ going from $t = 1$ to $t = 1.41$ ($\Delta E_{\text{PAO}}=0.001\text{Ry}$). If we now compare this result with our previously published results [32] obtained with plane-waves we notice that our present results give an e - t_2 splitting around 50meV less than the plane-wave splitting for both spins. This is roughly the same discrepancy found

for Δ_{FA} . As we have just shown, such a deviation from the plane-wave calculation cannot be lifted by increasing the size of the basis, since this does not produce variations larger than 2%. A possible origin of such a disagreement may be the slightly different pseudopotentials used.

In figure 4 we present the magnetization as a function of the lattice constant for MnAs and we compare it with that obtained previously in our plane-wave calculations [32]. The agreement is quite good; the transition to the

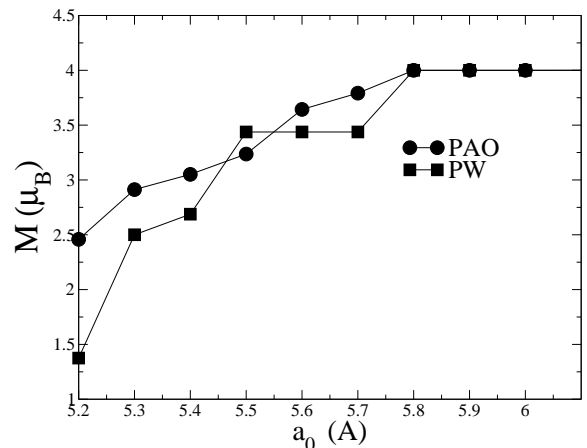


FIG. 4: Magnetization as a function of the lattice constant for zincblende MnAs.

half-metallic state is correctly predicted for $a_0=5.8\text{\AA}$ and also the dependence of the magnetization on the lattice spacing is well reproduced for $a_0 > 5.3\text{\AA}$. For smaller lattice spacings the two calculations disagree with a tendency of the PAO basis to over-stabilize the ferromagnetic phase. This is a quite general behavior that we found also with other basis sets. In particular for bases with a small number of ζ 's this effect is magnified. For instance the magnetization calculated with the first basis set of table II for $a_0 = 5.0\text{\AA}$ is $\sim 2.8\mu_B$, while that calculated with our optimized basis is $\sim 1.4\mu_B$. However we do not believe that our plane-wave and localized basis calculations should necessarily agree for strongly compressed unit cells since the portability of the two pseudopotentials used will be different.

Finally we check the ability of our optimized basis set to describe the electronic and structural properties of GaAs, which forms the matrix where the Mn ions are included in (Ga,Mn)As. We find an equilibrium lattice constant of $a_0=5.635\text{\AA}$ which is remarkably close to the experimental one. Moreover the bandstructure is very accurate; a comparison of our calculated eigenvalues with existing calculations is presented in table III.

In summary, we are confident that the results which we obtain using the numerical atomic orbitals method with the combination of Troullier-Martins pseudopotentials

tials and the basis set described in this section, are in good agreement with LSDA results obtained using other techniques.

III. ELECTRONIC CONFIGURATION OF GaAs:Mn

In this section we study the electronic structure of Mn in GaAs. We consider large GaAs cells (from 2 to 96 atoms) in which we replace one Ga atom with a Mn atom (Mn_{Ga}). We use 18 k points in the corresponding irreducible Brillouin zones for all the supercells and over 1000 k points for the primitive zincblende unit cell (2 atoms). Since the cell contains only one Mn atom and we use periodic boundary conditions the Mn atoms are forced to be ferromagnetically aligned. For the smaller cells (32 and 48 atoms) we perform several simulations changing the shape of the unit cell. This is equivalent to investigating different arrangements of the Mn atoms with respect to each other. We find that, although the general properties do not change, different Mn ion arrangements in the cell result in different total energies. For all the calculations we assume the GaAs experimental lattice spacing $a_0=5.65\text{\AA}$.

A. Partial DOS and charge density distribution

We start by analyzing the orbital-resolved density of states. In figure 5 we present as an example the DOS obtained for a 64 atom unit cell with one Mn_{Ga} substitution. Similar features are obtained for both higher and lower Mn concentrations. Far from the Fermi energy the DOS remains close to the DOS of GaAs (see figure 6), with a lower energy As- s band and the Ga(s)-As(p) valence band. At the Fermi energy the situation is markedly different. The majority spin band has a rather sharp peak, characteristic of a narrow band, while the minority spin has a gap. Such a band structure is the signature of a half-metallic material. The total magnetization of the cell is $4\mu_B$. Our calculations for higher and lower Mn concentrations show that the magnetization does not change with the Mn concentration. In the minority band the corresponding peak is shifted to higher energy and is very close to the edge of the GaAs conduction band. If we now consider the DOS projected onto the different orbital components of the wave-function and we look at the e and t_2 d -states of Mn some interesting features appear. The majority band exhibits two broad peaks between -4eV and -1eV below the Fermi energy with strong e and t_2 component respectively. In addition there is a rather narrow t_2 peak at the Fermi energy. In contrast the minority band has almost no d -character below E_F but instead has two sharp e and t_2 peaks around

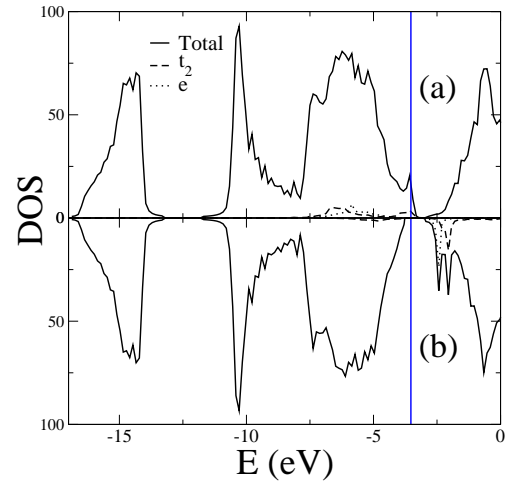


FIG. 5: Partial density of state for $\text{Ga}_{1-x}\text{Mn}_x\text{As}$ for $x = 0.3$ (one Mn_{Ga} in a 64 atom GaAs cell): (a) majority spin, (b) minority spin. The vertical line denotes the position of the Fermi energy. The dashed and dotted lines represent respectively the projection of the DOS onto the Mn- d t_2 and e orbitals.

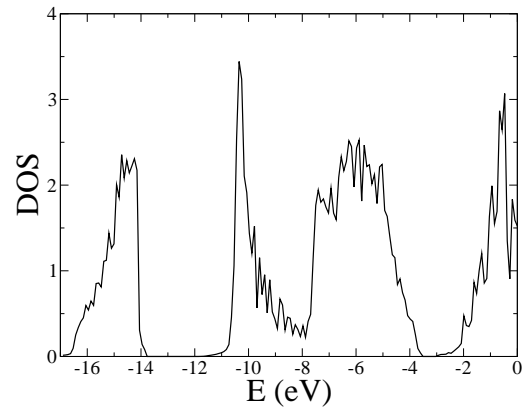


FIG. 6: DOS for GaAs.

1eV above E_F . The different peak widths reflect the different degrees of hybridization of the Mn- d band with the GaAs bands. The hybridization is much stronger for states far below the Fermi energy.

In order to have a better understanding of the p - d hybridization in diluted (Ga,Mn)As, we present in figure 7 the evolution of the Mn- d peaks as a function of the Mn concentration. The most relevant feature is that for the sharp peaks in both the majority and minority bands (columns (b) and (c)) the *relative* intensity of the d component of the DOS is independent of the Mn concentration. Therefore those portions of the DOS must be derived almost entirely from the Mn impurity and its four neighboring As atoms. This can also be seen by looking at the DOS projected onto the p states of the four atoms tetrahedrally coordinated with Mn (the dot-

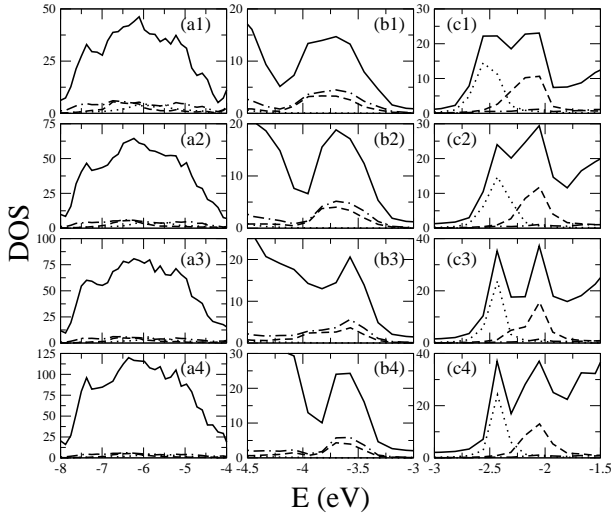


FIG. 7: Total and orbital-resolved DOS for different Mn concentrations. The three columns correspond to different energy regions and spins: (a) majority band between -4 and -1eV below E_F (broad Mn- d peaks), (b) majority band at the Fermi energy (sharp Mn- d peak), (c) minority band 1eV above E_F . The four rows indicate different Mn concentrations: (1) $x=0.06$ (1 Mn in 32 atoms), (2) $x=0.04$ (1 Mn in 48 atoms), (3) $x=0.03$ (1 Mn in 64 atom) and (4) $x=0.02$ (1 Mn in 96 atoms). The solid lines denote the total DOS while the dashed, dotted and dot-dashed lines denote the DOS coming respectively from the t_2 states of Mn, the e states of Mn, and the As(p) states of the four As atoms neighboring the Mn impurity. Note that the states of columns (b) and (c) do not scale with concentration, indicating strong local hybridization.

dashed line of figure 7). In summary our analysis shows that the MnAs_4 complex accounts for most of the DOS at the valence band edge for the majority band and at the conduction band edge for the minority.

In contrast the Mn- d states far below E_F results from strong coupling with the p orbitals of all the As atoms of the GaAs cell. This can be clearly seen in figure 8, where we present the charge density isosurface plots corresponding to the three DOS of figure 7. Figure 8 shows that the charge corresponding to states at the edge of the GaAs band gap is localized around the MnAs_4 complex (figures 8b and 8c), while the remaining Mn- d states are hybridized with all the As- p orbitals (figure 8a).

We now turn our attention to the distribution of the magnetization around the Mn ion. The magnetization around one atom placed at \mathbf{R}_0 is calculated as

$$M(R_i) = \int_{\Omega_{R_i}} [\rho_{\uparrow}(\mathbf{r} - \mathbf{R}_0) - \rho_{\downarrow}(\mathbf{r} - \mathbf{R}_0)] dr, \quad (2)$$

where Ω_{R_i} is a sphere of radius R_i and ρ_{σ} is the charge density for the spin σ . The charge density is calculated on a real-space grid by evaluating the localized orbitals on

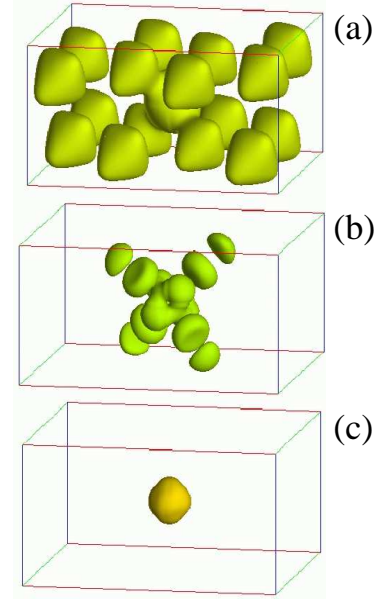


FIG. 8: Charge density isosurfaces for three states shown in figure 7. In this case we consider only $x=0.06$ (1 Mn in a cubic 32 atom cell). (a) Majority band between -4 and -1eV below E_F (broad Mn- d peaks), (b) majority band at the Fermi energy (sharp Mn- d peak), (c) minority band 1eV above E_F . The Mn ion is in the center of the cell.

such a grid [24]. Of course $M(R_i)$ depends on the cutoff radius R_i . In figure 9 we present the magnetization of Mn, and of the first and second As nearest neighbors of Mn, as a function of R_i .

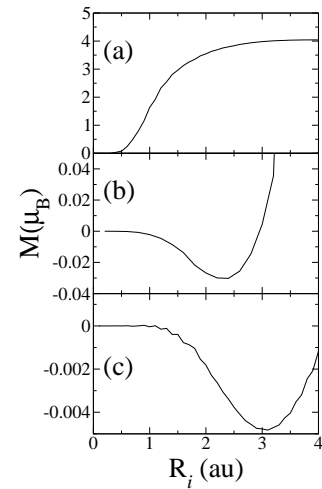


FIG. 9: Magnetization profile as a function of the integration radius R_i for (Ga,Mn)As with $x=0.3$ (1 Mn ion in a cubic 64 atom GaAs cell). (a) Mn, (b) first nearest As atom to Mn, (c) second nearest As atom to Mn.

In the case of Mn the magnetization saturates for $R_i=4.0$ au and remains almost constant up to $R_i \sim 18.0$ au when the next Mn shell is encountered. Hence we can easily deduce that the Mn magnetization is $4 \mu_B$ which is the saturation value. In contrast the magnetization around the As ions shows a negative minimum (between 2 and 3 au from the As ion, depending on the position of the As ion relative to the Mn ion) followed by a sharp increase. The minimum corresponds to a negative spin polarization with respect to the Mn and the following magnetization increase occurs at distances where the polarization of the neighboring atoms starts to be included in the integration. In the case of the first nearest neighbor this magnetization increase is due mainly to the spin polarization of Mn (figure 9b) and in the case of second nearest neighbors it is due to the four Ga ions coordinated to As (figure 9c). It is interesting to note that the polarization of the As ion is always negative with respect to that of Mn. This means that Mn and As are antiferromagnetically coupled. The values of the spin polarizations of As at the minima are $-0.03 \mu_B$ and $-0.005 \mu_B$ respectively for first and second nearest neighbors. These values of polarization are similar to those already published for GaAs/MnAs superlattices calculated with a first principle LMTO-ASA method [41]. It is worth noting that we did not find any sizeable changes in the magnetization per atom as a function of the Mn concentration for all the concentrations studied.

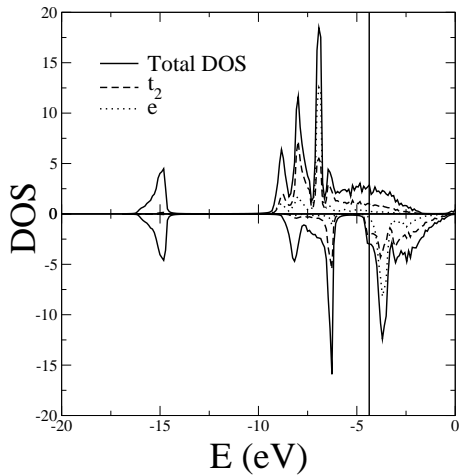


FIG. 10: Orbital resolved DOS for zincblende MnAs with lattice spacing $a_0 = 5.65 \text{ \AA}$. The vertical line denotes the position of the Fermi energy.

Finally we compare the orbital resolved DOS of (Ga,Mn)As with that of zincblende structure MnAs. In figure 10 we present the DOS for zincblende MnAs with the lattice spacing of GaAs (5.65 \AA), which is the same lattice spacing that we used for diluted (Ga,Mn)As. For

this lattice spacing MnAs is not an half-metal since the Fermi energy in the minority band cuts through the conduction band edge, mainly dominated by d electrons. Although the total DOS is different the projection onto the d -orbitals closely resembles that of diluted (Ga,Mn)As (see figure 5). In particular there is a large occupation of the d -orbitals in the majority band, while in the minority band only the bands of t_2 symmetry are occupied as a result of the hybridization with the As- p states at the edge of the valence band. The magnetization integrated around Mn ions is smaller in zincblende MnAs at this lattice constant than in (Ga,Mn)As. For a lattice spacing of $a_0=5.65 \text{ \AA}$ we find a Mn polarization of $3.79 \mu_B$, compared with $4.0 \mu_B$ of (Ga,Mn)As. In contrast the polarization of As in zincblende MnAs is considerably larger with an integrated magnetization of about $-0.17 \mu_B$. We also note that on increasing the lattice spacing the spin polarization of Mn increases, but the polarization of the As is largely unchanged. For instance at $a_0=5.80 \text{ \AA}$ we find $4.04 \mu_B$ and $-0.17 \mu_B$ respectively for the Mn and As magnetizations. This suggests that the polarization of Mn is related to the ionicity of the bond with As.

A more quantitative comparison of the zincblende MnAs with diluted (Ga,Mn)As can be obtained by performing Mülliken population analyses [42, 43]. We describe the results of such analyses in the next section.

B. Mülliken population analysis

We perform Mülliken population analyses [42, 43] in order to compare quantitatively the orbital occupations of (Ga,Mn)As at different dilutions. The Mülliken population analysis is a convenient way to separate different contributions to the total charge density. Suppose we have a system described by the wave-function $\phi = c_1\psi_1 + c_2\psi_2$, where ψ_α is a localized function and c_α is the corresponding amplitude. Then if the state ϕ is occupied by N electrons, the total occupation can be written as

$$N = Nc_1^2 + 2Nc_1c_2S_{12} + Nc_2^2, \quad (3)$$

where S_{12} is the overlap integral, $\int \psi_1\psi_2 dv$. Mülliken defined the sub-populations Nc_1^2 and Nc_2^2 as net populations and $2Nc_1c_2S_{12}$ as overlap population. Moreover if the overlap population is equally splitted between the two wavefunctions we obtain respectively $Nc_1^2 + Nc_1c_2S_{12}$ and $Nc_2^2 + Nc_1c_2S_{12}$, which are referred as gross populations. In what follows we always refer to the gross population. If the functions ψ_α represent orbital components of the angular momentum, then the populations correspond to orbital populations and the overlap population is the orbital overlap population. Similarly if the functions ψ_α are the atomic wave functions for the atom α then

we obtain the atomic populations and the atomic overlap population. We also define Mülliken atomic charge as the difference between the gross atomic charge (ie $eNc_2^2 + eNc_1c_2S_{12}$ with e the electronic charge) and the valence charge of the isolated atom. It is widely accepted that the absolute magnitude of the atomic charges can depend strongly on the basis set in which they are calculated [44]. However relative values of Mülliken populations can provide useful information when comparing different systems (for instance the amount of covalency in semiconductors) [45].

We start the analysis by calculating the Mülliken atomic charges for Ga, Mn and As in GaAs, MnAs and (Ga,Mn)As at different concentrations (table IV). In the case of (Ga,Mn)As for each atomic species we present the average values over the cell. Since we have already shown that the four As atoms coordinated with Mn (which we denote by As^{IV}) have quite different properties than the remaining As atoms, we calculate their average atomic charge separately. The table shows clearly the local character of the $MnAs_4$ center. We note that the average Mülliken charges of Ga and As closely resemble those of GaAs, particularly for low Mn concentrations. Of course in the extremely diluted limit GaAs:Mn one expects the average charges of Ga and As to be exactly those of GaAs. In contrast, the average Mülliken charge of the four As atoms coordinated with the Mn impurity does not change with concentration, confirming that the electronic structure of the $MnAs_4$ complex is not affected by the concentration. It is also interesting to note that these As atoms have small positive atomic charges whereas the other As atoms have negative atomic charge. A positive As atomic charge is also found in zincblende MnAs, although in that case its magnitude is much larger. The transition from GaAs:Mn to zincblende MnAs with increasing Mn concentration is reflected in the increase of Mülliken charge on the Mn atoms. Therefore the Mn-As bond becomes more ionic when the Mn concentration is increased. This picture, together with the almost complete occupation of the d shells in the majority band discussed in the previous section, is consistent with modeling Mn in GaAs as an A^0 impurity center composed of a negatively charged Mn ion in a d^5 configuration, and a weakly bound hole ($d^5 + h$) [46, 47]. The increase of Mn concentration, and the consequent increase of hole concentration, reduce the binding energy of the bound hole due to the partial screening of the potential. Therefore an increase of the Mülliken charge of Mn with concentration is expected. Nevertheless the agreement is only qualitative and a definitive prediction based solely on Mülliken analysis cannot be made.

We now turn our attention to the orbital population. In table V we present the orbital populations for the p orbitals of As and the d orbitals of Mn in MnAs and (Ga,Mn)As for both spin orientations. As before, we

distinguish between the As^{IV} atoms and the remaining As atoms. We do not report the orbital populations for Ga, for the s orbital of As and for the s and p orbitals of Mn since they are not relevant for the discussion.

Several important aspects can be pointed out from the table. The total population for the d orbital of Mn is around 5.5 electronic charges for all the systems studied. We do not expect integer values for the orbital population since strong $p-d$ hybridization is present. The total overlap population for zincblende MnAs is about 0.6 electronic charges and this can be considered to be the uncertainty on the determination of the orbital population. This give a Mn d orbital occupation of 4.6 ± 0.6 and 0.7 ± 0.6 for the majority and minority bands respectively. Although the orbital population is not an observable quantity and its absolute value may be affected by the choice of the basis set, we can conclude that the atomic configuration of Mn in GaAs is compatible with both $3d^5$ and $3d^6$. This is in agreement with recent x-ray absorption magnetic circular dichroism experiments [48], where the data are interpreted by assuming a Mn configuration consisting of 80% Mn $3d^5$ and 20% Mn $3d^6$. It is interesting to note that by decreasing the Mn concentration there is an increase of the polarization of the d orbital of Mn (the orbital population is enhanced in the majority band and reduced in the minority). This seems to be in favor of the $A^- 3d^5$ configuration in the limit of high dilution, as is reported extensively in the literature [46, 47, 49, 50, 51].

Table V also shows clearly that there is antiferromagnetic coupling between the Mn d and As p orbitals. The As p orbitals in fact have quite a large spin polarization opposite to that of Mn. This cannot be due to the overlap components of the orbital population, which would give the same polarization as that of Mn. It is also interesting to note that the spin polarization is much larger among the As^{IV} atoms for which it is almost insensitive to Mn concentration, than among the other As atoms. As expected it is still smaller than the As spin polarization in zincblende MnAs. Nevertheless we also see that the other As atoms have a small antiferromagnetic polarization of the p orbital, which decreases with concentration as expected. This is in very good agreement with the magnetization data presented in the previous section.

IV. EXCHANGE COUPLING

As we pointed out in the introduction, the evaluation of the exchange constant $N\beta$ is crucial for predicting the thermodynamic properties of (Ga,Mn)As. In this section we provide a theoretical estimate of the exchange constant and study its dependence on the Mn concentration. We begin by briefly describing the effect of the $sp-d$ exchange on the bandstructure of the host semiconductor

in the mean field approximation. Our starting point is the commonly used $sp-d$ exchange Hamiltonian [20]

$$H_{sp-d} = -\frac{1}{2} \sum_i \sum_{n, \mathbf{k}, \mathbf{k}'} J_n^{sp-d}(\mathbf{k}, \mathbf{k}') e^{i(\mathbf{k}-\mathbf{k}') \cdot \mathbf{R}_i} \mathbf{S}_i \times \left[\sum_{\mu\nu} c_{n\mathbf{k}\mu}^\dagger \sigma_{\mu\nu} c_{n\mathbf{k}'\nu} \right], \quad (4)$$

where $J_n^{sp-d}(\mathbf{k}, \mathbf{k}')$ is the exchange integral of the band electrons (n, \mathbf{k}) and (n, \mathbf{k}') with the Mn local spin \mathbf{S}_i , $c_{n\mathbf{k}}^\dagger$ and $c_{n\mathbf{k}}$ are the creation and annihilation operators for an electron in band n with Bloch vector \mathbf{k} . The sum extends over the valence ($n = v$) and conduction ($n = c$) bands of GaAs, and all the localized spins labelled by the index i . If we neglect interband terms which are negligible and replace the spin \mathbf{S}_i by the average spin $\langle S \rangle$ proportional to the magnetization we restore the translational invariance of the system. Therefore the expression (4) becomes diagonal in \mathbf{k} and can be written as a function of the Mn fraction x and the cation concentration N as

$$H_{sp-d} = -\frac{1}{2} x N \langle S \rangle \sum_k J_n^{sp-d}(k) (c_{n\mathbf{k}\uparrow}^\dagger c_{n\mathbf{k}\uparrow} - c_{n\mathbf{k}\downarrow}^\dagger c_{n\mathbf{k}\downarrow}), \quad (5)$$

with \uparrow (\downarrow) indicating the up spin (down spin) direction with respect to the mean field spin $\langle S \rangle$ and $J_n^{sp-d}(k) = J_n^{sp-d}(\mathbf{k}, \mathbf{k})$. If we now restrict our analysis to the band-edge (Γ point) and define $\alpha = J_c^{sp-d}(0)$ and $\beta = J_v^{sp-d}(0)$ we obtain the equations

$$\begin{aligned} H_{sp-d} &= -\frac{1}{2} x N \langle S \rangle \alpha (c_{c0\uparrow}^\dagger c_{c0\uparrow} - c_{c0\downarrow}^\dagger c_{c0\downarrow}) \\ H_{sp-d} &= -\frac{1}{2} x N \langle S \rangle \beta (c_{v0\uparrow}^\dagger c_{v0\uparrow} - c_{v0\downarrow}^\dagger c_{v0\downarrow}), \end{aligned} \quad (6)$$

for the conduction and valence bands respectively. We note that the same analysis can be carried out by assuming that the Mn impurities form a perfect ferromagnetic crystal. In such a case the derivation of equations (6) is identical to that given here if the magnetic moment per Mn atom is used for the mean field spin $\langle S \rangle$. Equation (6) relates the spin-splitting of the conduction and valence bands to the exchange integral calculated at $k = 0$. This quantity is usually extracted in optical magnetoabsorption experiments from the spin-splitting of the exciton lines. For instance the Zeeman splitting of the heavy hole exciton transition E_1 is

$$E_1 = x \langle S \rangle N (\beta - \alpha). \quad (7)$$

Other transitions give different combinations of α and β , which can then be determined. Note finally that the spin-splitting of both the valence and conduction bands in the mean field approximation is linear with the Mn concentration x .

We calculate the exchange constants directly from the conduction band-edge (valence band-edge) spin-splittings $\Delta E^c = E_\downarrow^c - E_\uparrow^c$ ($\Delta E^v = E_\downarrow^v - E_\uparrow^v$) as follows

$$N\alpha = \Delta E^c / x \langle S \rangle, \quad N\beta = \Delta E^v / x \langle S \rangle, \quad (8)$$

where $\langle S \rangle$ is half of the computed magnetization per Mn ion. In order to evaluate the parameters in equations (8) we compute the band structure around the Γ point for large GaAs cells with a single Mn impurity. In figure 11 we present as an example the results for a cubic cell containing 64 atoms. Since we are mainly interested in

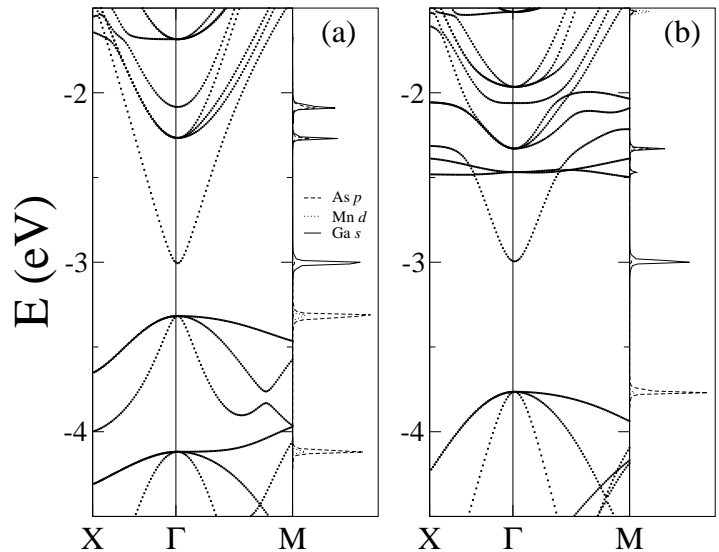


FIG. 11: Band structure and orbital resolved DOS at the Γ point for $\text{Ga}_{1-x}\text{Mn}_x\text{As}$ with $x=0.3$ (1 Mn ion in a cubic 64 atom GaAs cell): (a) majority band, (b) minority.

the Γ point we consider the band structure only along the direction $(\frac{1}{8}\frac{\pi}{c_0}, 0, 0) \rightarrow (0, 0, 0) \rightarrow (\frac{1}{8}\frac{\pi}{c_0}, \frac{1}{8}\frac{\pi}{c_0}, \frac{1}{8}\frac{\pi}{c_0})$ with c_0 the unit vector of the cubic cell. We indicate these two directions respectively as X and M. In figure 11 we also plot the orbital resolved DOS at the Γ point. This shows clearly that the valence band edge has mainly As- p character with contributions also from the t_2 Mn- d states due to hybridization, while the conduction band edge is formed by Ga- s states. In this way the spin-splitting is easily computed.

We consider different Mn concentrations and for the smaller unit cells (larger concentrations), different geometrical arrangements. We find that the spin-splittings of both the conduction and the valence bands are dependent on the relative positions between the Mn ions, with variations of up to 20%. In particular for the same Mn concentration we find large splittings when the Mn ions are clustered, and smaller splittings for homogeneously diluted systems. More details on the dependence of the exchange constant on the spatial arrangement of the Mn

ions will be published elsewhere [52]. In the following we consider only cells which maximize the separation between the Mn ions (uniform Mn distribution).

In figure 12 we present the spin-splitting for the conduction and for the valence band as a function of the Mn concentration and in table VI we list the corresponding exchange constants. Consider first the conduction band.

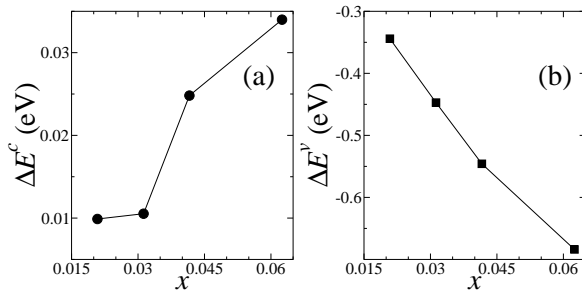


FIG. 12: Spin splitting of the conduction (a) and valence (b) bands as a function of the Mn concentration x for $\text{Ga}_{1-x}\text{Mn}_x\text{As}$. The corresponding exchange constants are listed in table VI.

Although the spin splitting shows large fluctuations with x , there is no systematic variation with the Mn concentration. With the caveat that DFT is a ground state theory and therefore does not describe accurately the conduction band, from table VI one can conclude that the coupling (s - d coupling) between the conduction band of GaAs and the Mn impurity is ferromagnetic. Also it is independent of x , as predicted by mean field theory, and has the value $N\alpha \sim 0.2$ eV. Note that ferromagnetic coupling is expected since in the case of the conduction band the only exchange is direct and also that the value of the exchange constant $N\alpha$ is very close to that usually found in II-VI semiconductors [53].

The situation is quite different for the valence band. First of all we see that the spin-splitting of the valence band edge is much larger than the typical absorption edge splitting in magnetooptical experiments [16]. For instance if we compare the results for $x = 0.032$ of reference [16] with those of figure 12 for the same concentration, we find that our calculated value is about four times larger than that obtained experimentally. However it is important to point out that in our calculation all the Mn ions contribute to the ferromagnetism. In contrast in real systems only a fraction of the Mn ions are ferromagnetically aligned, and the typical magnetization curves have a large paramagnetic component which does not saturate even at very high magnetic fields [54]. This has been confirmed by recent x-ray magnetic dichroism measurements [48]. Assuming a mean field picture, this suggests that the mean field spin calculated here is much larger than that present in actual samples. Turning the argument around we can conclude that our results are consistent

with experiments if we assume that in the latter the effective Mn concentration (contributing to the ferromagnetism) is only 1/4 of the nominal concentration.

A second important point is that, although figure 12b seems to suggest a linear behavior of the spin-splitting ΔE^c with x according to equation (6), a closer look at table VI reveals that the exchange constant $N\beta$ is strongly dependent on x . Specifically, $N\beta$ increases with decreasing Mn concentration, a behavior already well known to occur in $\text{Cd}_{1-x}\text{Mn}_x\text{S}$ [55, 56, 57]. This dependence of the exchange constant on x could be due to two possible reasons: i) the actual p - d coupling is not Kondo-like, or ii) the mean-field approximation that leads to equation (5) is not valid. Blinowski and Kacman studied the kinetic exchange interaction of various $3d$ metal impurities in zincblende semiconductors [58]. By applying canonical transformations to the p - d hybridization Hamiltonian [59] they evaluated the effective exchange interaction between the valence band and the d states of the impurity. They found that for the $3d^5$ and $3d^6$ configurations of the impurity the effective exchange has a Kondo-like form, while there are other non Kondo-like contributions for the $3d^4$ case. From the Mülliken analysis we can rule out this latter configuration, and conclude that the effective exchange is indeed Kondo-like. Therefore the dependence of $N\beta$ on x is suggestive of the breakdown of the mean-field approximation.

V. BREAKDOWN OF MEAN FIELD APPROXIMATION

The main hypothesis sustaining the mean field approximation is that the potential introduced by the Mn ions is weak with respect to the relevant band-width. This seems to be true in most of the II-VI semiconductors, however in the case of (Cd,Mn)S such a hypothesis breaks down and an apparent strong dependence of the exchange constant on the Mn concentration is found [55, 56, 57]. The case of Mn in GaAs looks very similar. We recall that for the very diluted limit there is some evidence of the Mn ion being able to bind a polarized hole [51]. This suggests that the potential created by Mn in GaAs may be strong and hence the mean field approximation breaks down.

Benoit à la Guillaume et al. [60] calculated the corrections to the mean field approximation using a free electron model, with the magnetic impurities described by square potentials. The energy was calculated within the Wigner-Seitz approach which is applicable only to the case of perfectly periodic crystal. Although the model has been refined [61, 62] the main findings are still valid. Here we illustrate briefly the model and we use it for computing the exchange constant.

We consider a free electron model with effective mass

m^* , and uniformly distributed magnetic impurities described by the potential

$$U(r) = W(r) - J(r)\mathbf{S} \cdot \mathbf{s}. \quad (9)$$

Here $W(r)$ is the spin independent substitutional potential and $J(r)$ is the p - d coupling between the free electron spin \mathbf{s} and the impurity spin \mathbf{S} . We further assume that $J(r)$ and $W(r)$ have the same square potential shape, and that all the impurity spins are ferromagnetically aligned. This leads to $U(r) = U_0 \theta(r - b)$ and also $U^{\uparrow(\downarrow)}(r) = (W \mp 5/4J)\theta(r - b)$, when $S = 5/2$ is considered. Finally the energy is calculated by solving a transcendental equation obtained by imposing the appropriate boundary conditions [60]. We define $\delta(x, U_0) = E(x, U_0)/E_{\text{mfa}}(x, U_0)$ as the deviation of the computed energy $E(x, U_0)$ from the mean field energy $E_{\text{mfa}}(x, U_0) = VNx$ where $V = \frac{4\pi}{3}b^3U_0$ and Nx is the Mn density. In figure 13 we present $\delta(x)$ as a function of x for different potentials $\eta = U_0/|U_c|$, where $U_c = -(\pi\hbar/2b)^2/2m^*$ is the binding potential. We no-

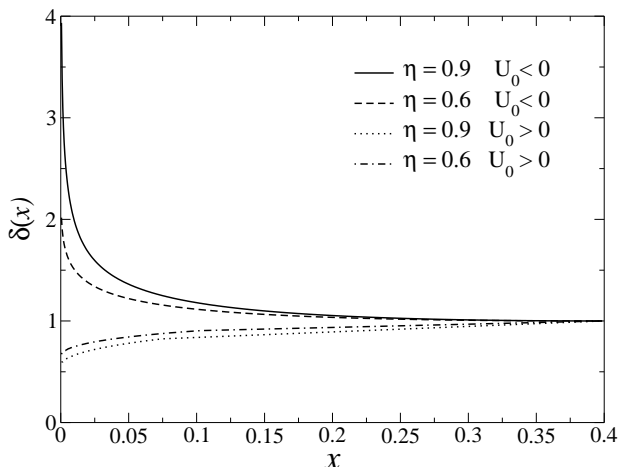


FIG. 13: Dependence of the correction factor $\delta(x)$ on the impurity concentration x for a range of potentials. Note that the deviation from mean field theory is larger for strongly attractive potentials.

tice that the corrections to mean field theory are large for small x and decrease with increasing x . In particular the mean field approximation breaks down when the potential is attractive and close to the binding potential ($\eta \rightarrow 1$), while it is reasonably good for repulsive potentials. We also note that the mean field approximation is recovered in both the limit of large Mn concentrations ($x \rightarrow 1$) and in the limit of weak potential ($\eta \rightarrow 0$). This general behavior can qualitatively explain our LDA results. Consider in fact the band edge spin-splitting

$$\Delta E^c(x) = \frac{4\pi b^3}{3} [(W + 5/4J)\delta(x, \eta^\dagger) -$$

$$(W - 5/4J)\delta(x, \eta^\uparrow)] Nx, \quad (10)$$

where $\eta^{\uparrow(\downarrow)} = (W \mp 5/4J)/|U_c|$. By comparing equation (10) with figure 13 one can see that for small x the spin-splitting is largely enhanced with respect to its mean field value. The deviation diminishes on increasing x , and vanishes in the limit of complete Mn substitution ($x = 1$). Note that the application of the mean field approximation at every x gives rise to an apparent increase of the exchange constant with the Mn concentration. This agrees with our LDA results.

It is also worth noting that the deviation from mean field theory is larger if the spin asymmetry of the potential U_0 is large. In particular the spin-splitting is largest when the potential is attractive for one spin species and repulsive for the other. In the opposite limit, when the mean field approximation is valid ($\delta \rightarrow 1$), the equation (10) reduces to the usual expression

$$\Delta E^c(x) = \frac{5}{2}N\beta x, \quad (11)$$

where we have defined the exchange constant $N\beta = N(4\pi b^3/3)J$.

In order to compare with experiments we perform a fit of our LDA data. We consider b , W and J as fitting parameters, with b varying between the cation-anion and the cation-cation distance and W and J chosen so that no bound holes are present. This last restriction takes into account the lack of any experimental evidence for bound holes at the concentrations investigated here. The

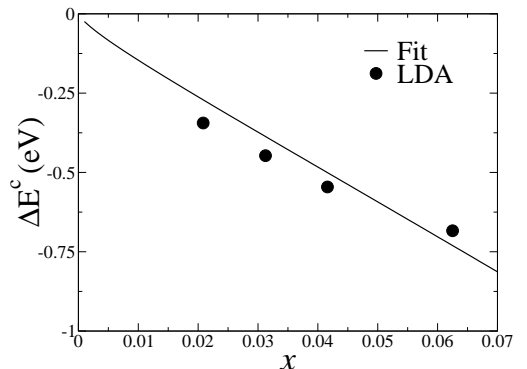


FIG. 14: Band edge spin-splitting: the circles represent our LDA data and the straight line the fit obtained with the model discussed in the text for the parameters $b = 3.6\text{\AA}$ $J = -1.05\text{eV}$ ($N\beta = -4.5\text{eV}$) and $W = -0.027\text{eV}$.

fitting procedure yields $b = 3.6\text{\AA}$ and $N\beta = -4.5\text{eV}$, although values in the range $3.6\text{\AA} < b < 3.9\text{\AA}$ and $-4.9\text{eV} < N\beta < -4.4\text{eV}$ fit equally well. It is important to note that for all the parameter sets which give a good fit one spin hole is nearly bound while the other feels a weak repulsive potential. Our best fit is presented in figure 14. Despite the roughness of the model the agreement

is reasonably good. It is interesting to point out that the model seems to underestimate the spin-splitting for small x and overestimate it for large x . This is not surprising; in the model we assume that the potential induced by the magnetic impurity does not depend on the impurity concentration. This is in general true for Mn in II-VI semiconductors, where Mn provides only a local spin. In the case of the III-V semiconductors, however, Mn acts both as an acceptor and as source of localized spins. Therefore it is natural to expect a progressive screening of the Mn potential with concentration due to the increase of the hole density. This effect, which is responsible for the lack of bound holes in low diluted (Ga,Mn)As, further reduces the deviation from the mean field approximation for large x , and better agreement with our LDA data may be found.

VI. CONCLUSIONS

We have investigated theoretically the magnetic properties of $\text{Ga}_{1-x}\text{Mn}_x\text{As}$ with dilutions ranging from $x=1$ to $x=0.02$. We found that Mn in GaAs has an atomic configuration compatible with both $3d^5$ and $3d^6$, and that the total occupation is not integer because of the strong p - d coupling with the valence band of GaAs. Such a coupling is antiferromagnetic with a remarkably large

exchange constant. We have shown that the exchange constant has an apparent dependence on the Mn concentration. This suggests that the generally used mean field approximation breaks down, since the potential induced by the Mn ions in GaAs cannot be treated perturbatively. Using a simple free-electron model we have calculated the corrections to the mean field expression for the spin-splitting of the GaAs valence band and found a good agreement with the LDA calculations. Further study is needed to determine the dependence of the spin-splitting on the confinement of the Mn ions in the case of highly ordered alloys.

Acknowledgments

This work made use of MRL Central Facilities supported by the National Science Foundation under award No. DMR96-32716. This work is supported by the DARPA/ONR under the grant N0014-99-1-1096, by ONR grant N00014-00-10557, by NSF-DMR under the grant 9973076 and by ACS PRF under the grant 33851-G5. P. O. acknowledges support from Fundaci3n Ram3n Areces (Spain). Useful discussions with N. Samarth, D.D. Awschalom and L.J. Sham are kindly acknowledged.

-
- [1] H. Ohno, H. Munekata, T. Penney, S. von Molnar and L.L. Chang, Phys. Rev. Lett. **68**, 2664 (1992)
 - [2] H. Ohno, A. Shen, F. Matsukura, A. Oiwa, A. Endo and S. Kutsumoto, Appl. Phys. Lett. **69**, 363 (1996)
 - [3] H. Ohno, J. Magn. Magn. Mater **200**, 110 (1999)
 - [4] H. Ohno, Science **281**, 951 (1998)
 - [5] G. Prinz, Phys. Today **48**, 58 (1995)
 - [6] J.M. Kikkawa and D.D. Awschalom, Phys. Rev. Lett. **80**, 4113 (1998)
 - [7] J.M. Kikkawa and D.D. Awschalom, Nature **397**, 139 (1998)
 - [8] Y. Ohno, D.K. Young, B. Beschoten, F. Matsukura and H. Ohno, D.D. Awschalom, Nature **402**, 790 (1999)
 - [9] G. Schmidt, D. Ferrand, L.W. Molenkamp, A.T. Filip and B.J. van Wees, Phys. Rev. B **62**, R4790 (2000)
 - [10] D.P. Di Vincenzo, Science **270**, 255 (1995)
 - [11] T. Dietl, H. Ohno, F. Matsukura, J. Cib3rt and D. Ferrand, Science **287**, 1019 (2000)
 - [12] T. Dietl, H. Ohno and F. Matsukura, cond-mat/0007190
 - [13] H. Akai, Phys. Rev. Lett. **81**, 3002 (1998)
 - [14] J. Szczytko, W. Mac, A. Stachow, A. Twardowski, P. Becla and J. Tworzyclo, Solid State Commun. **99**, 927 (1996)
 - [15] K. Ando, T. Hayashi, M. Tanaka and A. Twardowski, J. Appl. Phys. **83**, 6548 (1998)
 - [16] J. Szczytko, W. Mac, A. Twardowski, F. Matsukura and H. Ohno, Phys. Rev. B **59**, 12935 (1999)
 - [17] F. Matsukura, H. Ohno, A. Shen and Y. Sugawara, Phys. Rev. B **57**, R2037 (1998)
 - [18] T. Omiya, F. Matsukura, T. Dietl, Y. Ohno, T. Sakon, M. Motokawa and H. Ohno, Physica E **7**, 976 (2000)
 - [19] J. Okabayashi, A. Kimura, O. Rader, T. Mizokawa, A. Fujimori, T. Hayashi and M. Tanaka, Phys. Rev. B **58**, R4211 (1998)
 - [20] B.E. Larson, K.C. Hass, H. Ehrenreich and A.E. Carlson, Phys. Rev. B **37** 4137 (1988)
 - [21] J. Szczytko, W. Mac, A. Stachow, A. Twardowski, P. Becla and J. Tworzyclo, Solid State Commun. **99**, 927 (1996)
 - [22] H. Hohenberg and W. Kohn, Phys. Rev. **136**, B864 (1964), W. Kohn and L. Sham, Phys. Rev. **140** A1133 (1965)
 - [23] P. Ordej3n, D. S3nchez-Portal, E. Artacho and J.M. Soler, SIESTA, Spanish Initiative for Electronic Simulations with Thousands of Atoms
 - [24] D. S3nchez-Portal, P. Ordej3n, E. Artacho and J.M. Soler, Internat. J. Quantum Chem. **65**, 453 (1997) and references therein
 - [25] P. Ordej3n, Phys. Stat. Sol. B **217**, 335 (2000)
 - [26] D.M. Ceperley and B.J. Alder, Phys. Rev. Lett. **45**, 566 (1980)
 - [27] P. Pulay, Chem. Phys. Lett. **73**, 393 (1980)

- [28] N. Troullier and J.L. Martins, Phys. Rev. B **43**, 1993 (1991)
- [29] S.G. Louie, S. Froyen and M.L. Cohen, Phys. Rev. B **26**, 1738 (1982)
- [30] L. Kleinman and D.M. Bylander, Phys. Rev. Lett. **48**, 1425 (1982)
- [31] G. Theurich, private communication. The calculations have been performed with the code SPINOR which is a general-spin implementation of density functional theory including spin-orbit interaction written in C. The code is publically available at <http://www.mrl.ucsb.edu/~theurich/Spinor/>
- [32] S. Sanvito and N.A. Hill, cond-mat/0004184 to be published on Phys. Rev. B
- [33] E. Artacho, D. Sanchez-Portal, P. Ordejón, A. García and J.M. Soler, Phys. Stat. Sol. **215**, 809 (1999)
- [34] O.F. Sankey and D.J. Niklewski, Phys. Rev. B **40**, 3979 (1989)
- [35] J. Izquierdo, A. Vega, L. C. Balbás, D. Sánchez-Portal, J. Junquera, E. Artacho, J. M. Soler and P. Ordejón, Phys. Rev. B **61**, 13639 (2000)
- [36] M. Calleja, C. Rey, M.M.G. Alemany, L.J. Gallego, P. Ordejón, D. Sánchez-Portal, E. Artacho and J.M. Soler, Phys. Rev. B **60**, 2020 (1999)
- [37] C. Filippi, D.J. Singh and C.J. Umrigar Phys. Rev. B **50**, 14947 (1994)
- [38] V. Fiorentini, Phys. Rev. B **46**, 2086 (1992)
- [39] R.W. Jansen and O.F. Sankey, Phys. Rev. B **36**, 6520 (1987)
- [40] O. Madelung, *Semiconductors, Group IV Elements and III-V Compounds*, Landolt-Börnstein, New Series, Vol. 17, Pt. a (Springer-Verlag, Berlin, 1991)
- [41] T. Ogawa, M. Shirai, N. Suzuki and I. Kitagawa, J. Magn. Magn. Mater. **196-197**, 428 (1999)
- [42] R.S. Mülliken, J. Chem. Phys. **23**, 1833 (1955)
- [43] R.S. Mülliken, J. Chem. Phys. **23**, 1841 (1955)
- [44] E.R. Davidson and S. Chakravorty, Theor. Chim. Acta **83**, 319 (1992)
- [45] M.D. Segall, R. Shah, C.J. Pickard and M.C. Payne, Phys. Rev. B **54**, 16317 (1996)
- [46] J. Schneider, U. Kaufmann, W. Wilkening, M. Baeumler and F. Köhl, Phys. Rev. Lett. **59**, 240 (1987)
- [47] A. Twardowski, Mater. Sci. Eng. B **63**, 96 (1999)
- [48] H. Ohldag, V. Solinus, F.U. Hillebrecht, J.B. Goedkoop, M. Finazzi, F. Matsukura and H. Ohno, Appl. Phys. Lett. **76**, 2928 (2000)
- [49] A.K. Bhattacharjee, C. Benoit à la Guillaume, Solid State Commun. **113**, 17 (2000)
- [50] V.F. Sapega, T. Ruf and M. Cardona, Solid State Commun. **114**, 573 (2000)
- [51] M. Linnarsson, E. Janzén, B. Monemar, M. Kleverman and A. Thilderkvist, Phys. Rev. B **55**, 6938 (1997)
- [52] S. Sanvito and N.A. Hill, in preparation
- [53] *Diluted Magnetic Semiconductors*, edited by J.K. Furdyna and J. Kossut, Semiconductor and Semimetals Vol. 25 (Academic, New York, 1988); *Diluted Magnetic Semiconductors*, edited by M. Balkanski and M. Averous (Plenum, New York, 1991)
- [54] A. Oiwa, S. Kutumoto, A. Endo, M. Hirasawa, Y. Iye, H. Ohno, F. Matsukura, A. Shen and Y. Sugawara, Solid State Commun. **103**, 209 (1997)
- [55] V.G. Abrammishvili, S.I. Gubarev, A.V. Komarov and S.M. Ryabchenko, Fiz. Tverd. Tela **26**, 1095 (1984) [Sov. Phys. Solid State **26**, 666 (1984)]
- [56] S.I. Gubarev and M.G. Tyazhlov, Fiz. Tverd. Tela **32**, 635 (1990) [Sov. Phys. Solid State **32**, 373 (1990)]
- [57] S.I. Gubarev and M.G. Tyazhlov, Pis'ma Zh. Eksp. Teor. Fiz. **44**, 385 (1986) [JEPT Lett. **44**, 494 (1986)]
- [58] J. Blinowski and P. Kacman, Phys. Rev. B **46**, 12298 (1992)
- [59] R.H. Parmenter, Phys. Rev. B **8**, 1273 (1973)
- [60] C. Benoit à la Guillaume, D. Scalbert and T. Dietl, Phys. Rev. B **46**, 9853 (1992)
- [61] D. Scalbert, A. Ghazali and C. Benoit à la Guillaume, Phys. Rev. B **48**, 17752 (1993)
- [62] J. Tworzydło, Phys. Rev. B **50**, 14591 (1994)

GaAs	Γ_1	Γ_1	X_1	X_3	X_5	X_1	L_2	L_1	L_3	L_1
PAO _{exp}	-12.91	0.57	-10.53	-7.05	-2.84	1.71	-11.25	-6.86	-1.26	1.34
PAO _{the}	-12.99	0.66	-10.56	-7.10	-2.88	1.88	-11.30	-6.92	-1.27	1.39
LAPW [37]	-12.80	0.29	-10.29	-6.89	-2.69	1.35	-11.03	-6.70	-1.15	0.85
PW-PP [38]	-12.56	0.55	-10.25	-6.70	-2.58	1.43	-10.95	-6.52	-1.09	1.02
LDA-PAO [39]	-12.38	1.03	-9.85	-6.72	-2.66	1.59	-10.63	-6.53	-1.14	1.28
EXP [40]	-13.10	1.63	-10.75	-6.70	-2.80	2.18	-11.24	-6.70	-1.30	1.85

TABLE III: Kohn-Sham eigenvalues calculated using various methods. The energies are calculated with respect to the top of the valence band and all the units are eV. PAO_{exp} and PAO_{the} are the results of the present calculation assuming the lattice constant to be respectively the experimental $a_0 = 5.65\text{\AA}$ and the theoretical $a_0 = 5.635\text{\AA}$.

Material	Ga ($ e $)	Mn ($ e $)	As ($ e $)	As ^{IV} ($ e $)
GaAs	+0.056		-0.056	
MnAs		-0.322	+0.332	
Ga _{0.938} Mn _{0.062} As	+0.042	-0.089	-0.046	+0.005
Ga _{0.958} Mn _{0.042} As	+0.046	-0.085	-0.049	+0.005
Ga _{0.969} Mn _{0.031} As	+0.047	-0.083	-0.049	+0.005
Ga _{0.979} Mn _{0.021} As	+0.049	-0.086	-0.050	+0.005

TABLE IV: Mülliken atomic charges for GaAs, MnAs and (Ga,Mn)As at different Mn concentrations. The last two columns correspond respectively to the average over the As atom excluding the ones coordinated with Mn and the average over the four As atoms coordinated with Mn. The lattice spacing of MnAs is assumed to be $a_0 = 5.65\text{\AA}$.

Material	Mn- d_\uparrow ($ e $)	Mn- d_\downarrow ($ e $)	As- p_\uparrow ($ e $)	As- p_\downarrow ($ e $)	As ^{IV} - p_\uparrow ($ e $)	As ^{IV} - p_\downarrow ($ e $)
MnAs	4.642	0.855	1.365	1.650		
Ga _{0.938} Mn _{0.062} As	4.665	0.788	1.626	1.637	1.580	1.647
Ga _{0.958} Mn _{0.042} As	4.679	0.770	1.628	1.638	1.583	1.644
Ga _{0.969} Mn _{0.031} As	4.675	0.771	1.630	1.637	1.584	1.644
Ga _{0.979} Mn _{0.021} As	4.682	0.768	1.632	1.636	1.584	1.644

TABLE V: Mülliken atomic orbital populations in MnAs and (Ga,Mn)As at different Mn concentrations. The symbols \uparrow and \downarrow correspond to majority and minority spin respectively. The last two columns correspond to the four As atoms coordinated with Mn. The lattice spacing of MnAs is assumed to be $a_0 = 5.65\text{\AA}$.

x	$N\alpha$ (eV)	$N\beta$ (eV)
1.0	0.176	-2.44
0.06250	0.272	-5.48
0.04166	0.298	-6.54
0.03125	0.168	-7.34
0.02084	0.234	-8.16

TABLE VI: Exchange constants as a function of the Mn concentration x for Ga_{1-x}Mn_xAs.